Supporting Information

10 Gbit·s^{-1} free space data transmission at 9 μm wavelength with unipolar quantum optoelectronics

Hamza Dely[+], *Thomas Bonazzi*[+], *Olivier Spitz, Etienne Rodriguez, Djamal Gacemi, Yanko Todorov, Konstantinos Pantzas, Grégoire Beaudoin, Isabelle Sagnes, Lianhe Li, Alexander Giles Davies, Edmund H. Linfield, Frédéric Grillot, Angela Vasanelli, Carlo Sirtori**

+ These authors contributed equally to this work

Simulation of the electronic states of the Stark modulator and of the quantum cascade detector

The electronic states of the heterostructures are numerically calculated by using a three-band Kane model in the envelope function approximation, following reference.[1]

A) Stark modulator

Figure S1 presents the conduction band profile and the square moduli of the electronic envelope functions, plotted at the corresponding energies. Three electronic bound states are found, whose energies at zero bias are: 95 meV (state 1), 256 meV (state 2) and 359 meV (state 3). Only states 1 and 2 contribute to the absorption of the laser beam at 9 μm, while transition 1-3 is at ~5 μm. The sample is doped 1.5x10^{18} cm^{-3} in the large well, so that the Fermi energy is located below state 2 and we can consider that only state 1 is occupied. Electrons are thus mainly localized in the first well, and tunnelling and escape probability are negligible in the entire range of applied bias.

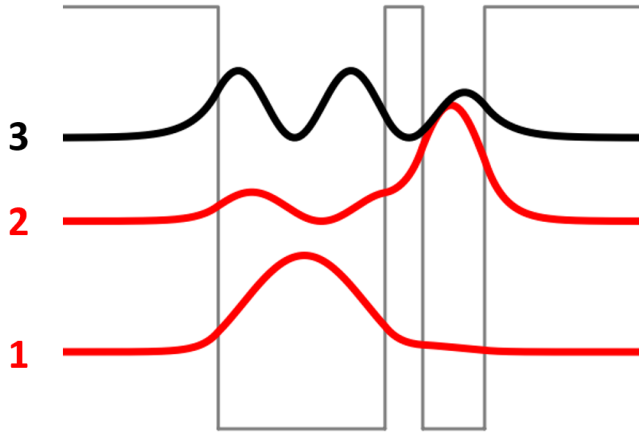

Figure S1. Conduction band profile and square moduli of the electronic envelope functions of the Stark modulator.

B) Quantum cascade detector

Figure S2 presents the conduction band profile of one period of our quantum cascade detector (QCD), together with the square moduli of the electronic envelope functions plotted at the corresponding energies. The design of the active region is based on a diagonal transition:[2] light emitted by the laser photoexcites electrons through absorption between the states 1 and 2, plotted in red. Photoexcited electrons are then extracted through the cascade towards the ground state of the following period by longitudinal optical phonon scattering. This type of design typically yields a lower absorption than its vertical counterpart. The decrease in the oscillator strength is compensated by an improved extraction efficiency through the cascade, thanks to the delocalization of state 2 in the extraction region.

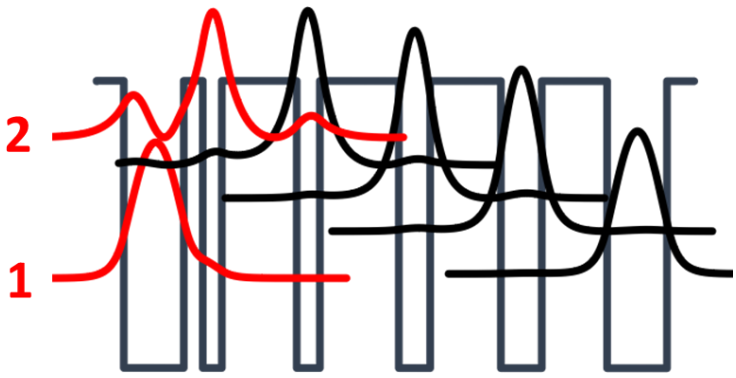

Figure S2: Conduction band diagram of the active region of the GaAs/AlGaAs diagonal QC detector, together with the square moduli of the relevant envelope functions plotted at the corresponding energies.

Linearity of the Stark modulator

The operation of the Stark modulator was characterized by studying the detected power as a function of the electrical power on the modulator (**Figure S3**). The modulator was operated

close to the inflexion point of the transmittance function (**Figure 3d** of the main text), and biased with a DC voltage of 2.05 V and with a sinusoidal voltage $V = V_m \cos(\omega t)$ at a fixed frequency of 12 MHz. The measured photocurrent, from which we extracted the detected optical power, is proportional to the absorbance $\alpha(V)$. Through Taylor expansion of $\alpha(V)$ around the inflexion point, we found that the detected optical power up to the third order in V can be written as:

$$P(V_m) = P_0\,(1 - m(V_m)\cos(\omega t) + l(V_m)\cos(3\omega t))$$

In this expansion, m is the sideband-to-carrier intensity ratio. The third order allows quantifying the non-linearity of the modulator through the calculation of the input third-order intercept point (IIP3), which was found to be equal to 18 dBm, corresponding to an applied bias of 44 V on our 80 x 80 µm² modulator. Even at large biases covering a large part of the absorption range, this third harmonic lies 20 dB below the fundamental. The input 1 dB compression point (P1dB), where the output signal is 1dB below its linear regime value, is 5.75 dBm (9.5 V). From these observations we can conclude that operating the modulator up to 9 V keeps the device in its linear regime and does not lead to a significant distortion in the modulated signal.

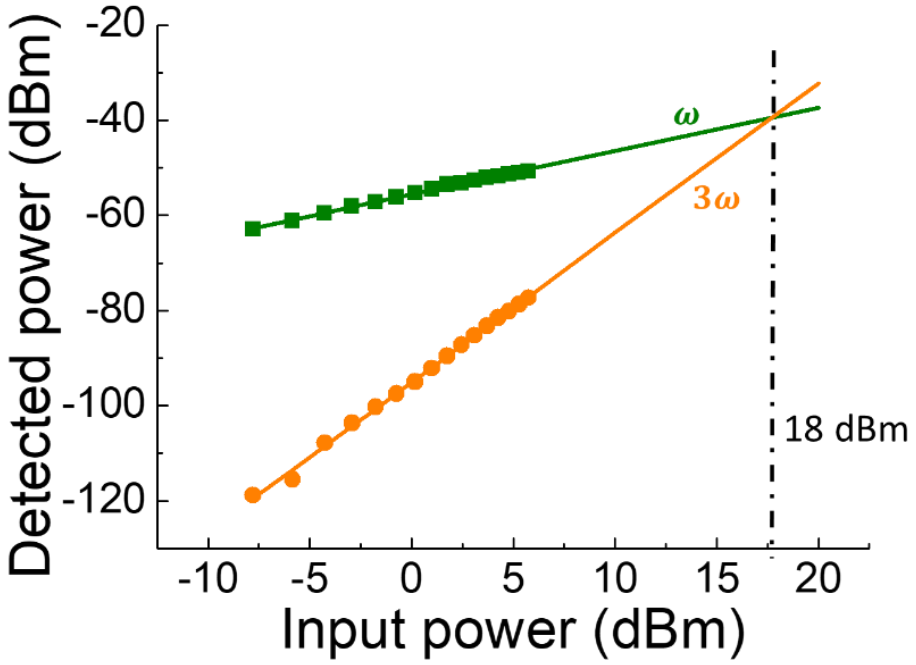

Figure S3. Detected power as a function of the electrical power at the modulation frequency ω (green) and at 3ω (orange).

Electrical power dissipated by the modulator

Figure S4 presents the power dissipated by the modulator as a function of the applied bias, as extracted for each device from the Current-Voltage characteristics measured with Keithley 2450.

For our data transmission experiment, we used a 7 Vpp square signal centered around 1.1 V DC. At this voltage the modulator dissipated approximately 1 pJ/bit. This energy per bit is comparable to state-of-the-art modulation even in the telecom wavelengths.[3]

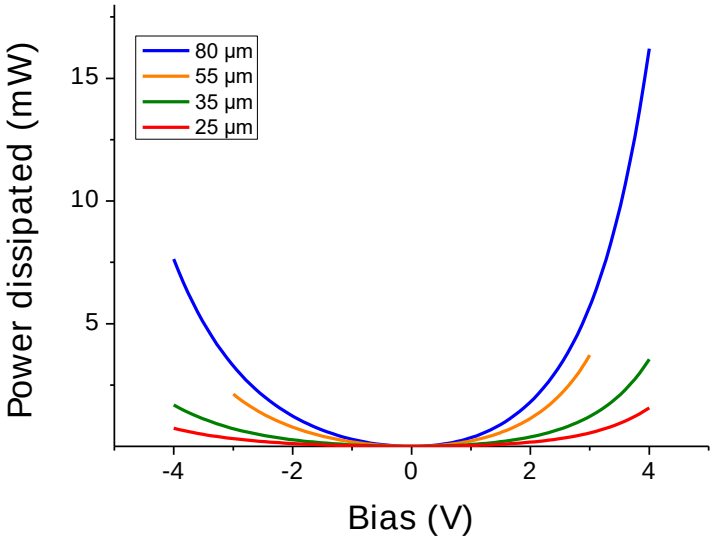

Figure S4. Electrical power dissipated by the modulator as a function of the applied bias for four devices with different size of the square mesa.

Rectification measurements on the Stark modulator

Rectification measurements were realized on the Stark modulators using a 40 GHz RF probe. This measurement allows extracting the intrinsic bandwidth of the devices without the parasitic capacitance of the PCB mount. **Figure S5** shows the normalized rectified current for four different sizes of the mesa. The four devices exhibit a flat response up to their cutoff and behave like first-order devices (-20 dB/decade) above this point. Note that there is no resonance due to relaxation oscillations near the frequency cutoff, as expected for a unipolar device.

From these measurements we extracted the cutoff frequencies of the four devices, that are plotted in the inset to **Figure S5** (symbols) as a function of the inverse of the device surface. The blue line shows the calculated cutoff frequency only considering the size of the devices, while the orange line includes a parasitic capacitance of 61 fF.

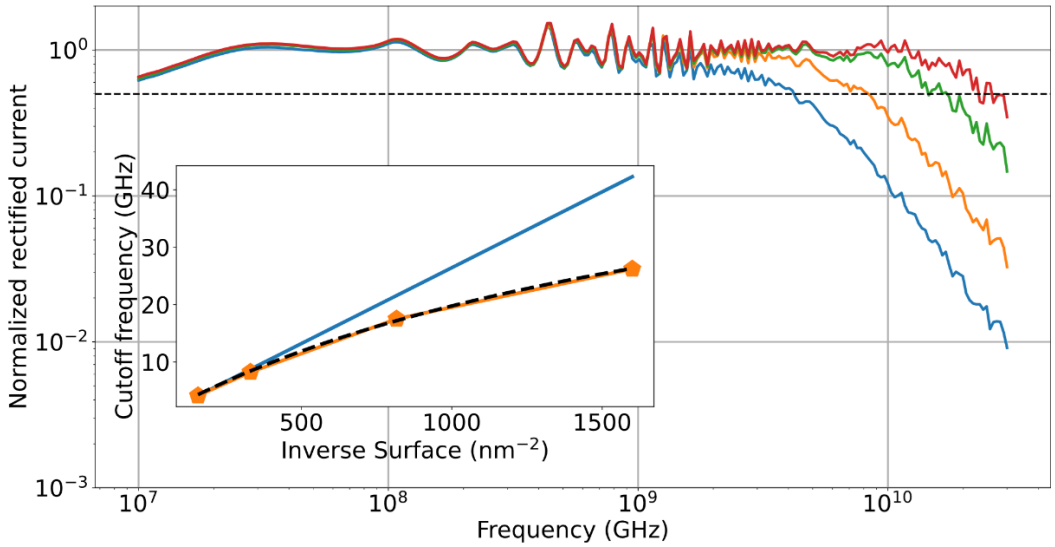

Figure S5. Rectification measurements of Stark modulators with different sizes: 80 x 80 µm² (blue curve), 55 x 55 µm² (orange), 35 x 35 µm² (green) and 25 x 25 µm² (red). The inset presents the cut-off frequency as a function of the device size (symbols), simulated by only including the geometric capacitance of the device (orange continuous line) and considering an extra capacitance of 61 fF, due to non-ideal capacitance effects for small-devices (black dashed line).

References

1. Sirtori, C., Capasso, F., Faist, J., et Scandolo, S. (1994) Nonparabolicity and a sum rule associated with bound-to-bound and bound-to-continuum intersubband transitions in quantum wells. *Physical Review B*, **50** (12), 8663-8674.
2. Reininger, P., Schwarz, B., Detz, H., MacFarland, D., Zederbauer, T., Andrews, A.M., Schrenk, W., Baumgartner, O., Kosina, H., et Strasser, G. (2014) Diagonal-transition quantum cascade detector. *Appl. Phys. Lett.*, **105** (9), 091108.
3. Yamaoka, S., Diamantopoulos, N.-P., Nishi, H., Nakao, R., Fujii, T., Takeda, K., Hiraki, T., Tsurugaya, T., Kanazawa, S., Tanobe, H., Kakitsuka, T., Tsuchizawa, T., Koyama, F., et Matsuo, S. (2021) Directly modulated membrane lasers with 108 GHz bandwidth on a high-thermal-conductivity silicon carbide substrate. *Nature Photonics*, **15** (1), 28-35.